Geophysical Research Letters

RESEARCH LETTER
10.1029/2024GL112543

Circulation and Cloud Responses to Patterned SST Warming

Anna Mackie[1], Michael P. Byrne[1,2], Emily K. Van de Koot[2], and Andrew I. L. Williams[3]

[1]School of Earth and Environmental Sciences, University of St Andrews, St Andrews, UK, [2]Atmospheric, Oceanic and Planetary Physics, University of Oxford, Oxford, UK, [3]Program in Atmospheric and Oceanic Sciences, Princeton University, Princeton, NJ, USA

Key Points:

- Direct warming of ascent regions leads to their areal contraction while warming in regions of descent has little effect on ascent fraction
- We develop a metric relating near-surface and free tropospheric moist static energies to ascent fraction accounting for dry air entrainment
- Our metric reveals the contributions of different circulation regimes to warming-induced changes in cloud radiative effect

Supporting Information:

Supporting Information may be found in the online version of this article.

Correspondence to:

A. Mackie,
arm33@st-andrews.ac.uk

Citation:

Mackie, A., Byrne, M. P., Van de Koot, E. K., & Williams, A. I. L. (2025). Circulation and cloud responses to patterned SST warming. *Geophysical Research Letters*, *52*, e2024GL112543. https://doi.org/10.1029/2024GL112543

Received 13 SEP 2024
Accepted 27 MAR 2025

Author Contributions:

Conceptualization: Anna Mackie, Michael P. Byrne, Emily K. Van de Koot, Andrew I. L. Williams
Formal analysis: Anna Mackie
Methodology: Anna Mackie, Michael P. Byrne, Emily K. Van de Koot, Andrew I. L. Williams
Visualization: Anna Mackie
Writing – original draft: Anna Mackie
Writing – review & editing: Anna Mackie, Michael P. Byrne, Emily K. Van de Koot, Andrew I. L. Williams

Abstract The climatological atmospheric circulation is key to establishing the tropical "pattern effect", whereby cloud feedbacks induced by sea surface temperature (SST) warming depend on the spatial structure of that warming. But how patterned warming-induced circulation changes affect cloud responses is less clear. Here we use idealized simulations with prescribed SST perturbations to understand the contributions to changes in tropical-mean cloud radiative effects (CRE) from different circulation regimes. We develop a novel framework based on moist static energy to understand the circulation response, targeting in particular the bulk circulation metric of ascent fraction. Warming concentrated in regions of ascent leads to a strong "upped-ante" effect and spatial contraction of the ascending region. Our framework reveals substantial contributions to tropical-mean CRE changes not only from traditional "pattern effect" regimes, but also from the intensification of convection in ascent regions as well as a smaller contribution from cloud changes in convective margins.

Plain Language Summary Recent advances have demonstrated the importance of spatial patterns in tropical sea surface warming for determining how Earth's tropical energy balance responds to climate change. Sensitivity of the energy balance is higher when warming is concentrated in regions where air is generally ascending, such as the west Pacific, than in regions where air is generally descending, such as in the east Pacific. This variation in sensitivity across regions depends on the degree to which surface warming is communicated to the upper atmosphere, and subsequently whether low clouds brighten in the east Pacific. What is less well understood is how the atmospheric circulation—the movement of air—responds to these surface warming patterns, and how these circulation changes may be coupled to clouds and energy balance. Using climate simulations where only a specified patch of the tropical ocean is warmed, we demonstrate that if ascent regions are directly warmed these regions tend to contract in area. But there is little change in circulation if descent regions are warmed. We develop a simple conceptual model which provides insight into the mechanisms of these circulation changes and demonstrate that cloud changes can be decomposed into the responses from individual circulation regimes.

1. Introduction

Recent work has established the importance of spatial patterns in tropical sea surface temperature (SST) warming for cloud feedbacks and thus estimates of climate sensitivity (Andrews et al., 2018; Armour et al., 2024; Dong et al., 2019; Zhou et al., 2016). This "pattern effect" encompasses a broad range of feedbacks induced by patterned SST warming, with strong emphasis in the literature on the influence of SST warming patterns on low clouds in regions of climatological subsidence (e.g., Andrews & Webb, 2018; Fueglistaler, 2019; Rugenstein et al., 2023). However, changes in other cloud regimes may also be important. For example, previous work has shown significant correlations between observed relative SST warming and local longwave cloud effects (Mackie et al., 2021). Furthermore, focusing on cloud responses in climatological circulation regimes neglects potential changes to those regimes, with potentially important implications for how the pattern effect evolves in a changing climate. GCM projections suggest a variety of tropical circulation responses to warming, including a weaker Walker circulation (e.g., Duffy & O'Gorman, 2023; Wills et al., 2022); and narrowing and strengthening of the ITCZ (Byrne et al., 2018; Byrne & Schneider, 2016). Some of these circulation changes directly influence tropical cloud feedbacks (Bony et al., 2004; Byrne & Schneider, 2018; Hill et al., 2023; Mackie & Byrne, 2023; Wyant et al., 2006), but their importance for the pattern effect specifically is less clear.

Recently, A. I. L. Williams et al. (2023), hereafter W23, showed that the ability of patterned SST warming to influence free tropospheric MSE—and thus induce remote cloud changes—is dependent on whether the sub-cloud layer is convectively coupled to the free troposphere in the warmed region. This framework is based on two central concepts: First, convective quasi-equilibrium (CQE) suggests that saturation MSE in the free troposphere co-varies with sub-cloud MSE in regions of deep convection (Emanuel et al., 1994). Second, the weak temperature gradient (WTG) approximation suggests that temperature and therefore saturation MSE in the tropical free troposphere are constrained by gravity waves to be roughly spatially uniform due to a weak Coriolis force (Sobel & Bretherton, 2000).

Here we extend the MSE framework put forward by W23 to examine changes in tropical cloud radiative effect in different circulation regimes in response to localized SST warming and cooling. Section 2 introduces the simulations to be analyzed. Section 3 examines the circulation changes induced by localized SST perturbations in different regions and presents an MSE framework to interpret the responses. This framework is applied to understand and quantify cloud responses in different circulation regimes in Section 4 before discussion in Section 5.

2. Simulations

We analyze simulations from an atmosphere-only configuration of the ICON GCM (Giorgetta et al., 2018) from W23, where we refer the reader to for more detailed information. We use a 20-year control simulation forced with monthly climatologies of SST and sea-ice averaged over 1979–2016 (Neale & Hoskins, 2000). SST perturbations in different locations are then applied using a "cosine patch" approach, following Barsugli and Sardeshmukh (2002). We analyze simulations with perturbation patches centered on the equator at 100°E, 140°E, 180°E and 220°E [see Figure 2a from W23]. For each patch, 8 different SST perturbations are analyzed (maximum −4 K to +4 K in 1 K increments), with each perturbation simulation run for 10 years (due to computational constraints). We use 19-year and 9-year climatological monthly means in our analyses for the control and perturbation simulations, respectively, having discarded the first year of all simulations as spin-up. We define our domain as ocean-only points between 20°S and 20°N.

We assess changes in large-scale circulation with warming via ascent fraction (denoted α). Ascent fraction is calculated using the area-weighted fraction of the domain which is ascending as defined by simulated vertical velocity at 500 hPa.

3. Moist Static Energy Framework for Ascent Fraction

In Figure 1 we show the response of ascent fraction (α) to SST patch warming in different locations. For the three patches which are located in regions which are generally ascending in the free troposphere (100°E, 140°E, and 180°E; see Figures S1a–S1c in Supporting Information S1), SST warming leads to a spatial contraction of the ascent regions (red lines, Figures 1a–1c). The contraction of ascent under warming is described by the upped-ante mechanism (Neelin et al., 2003), whereby higher free-tropospheric MSE represents an increase in the magnitude of sub-cloud MSE required to maintain convective coupling, known as the convective threshold. This increased threshold can be reached in the core of convective regions but not at the convective margins, where advection of low-MSE air from subsidence regions suppresses increases in sub-cloud MSE. SST cooling has a weaker influence but also leads to a contraction in ascent region. This contraction is the net effect of two competing influences: firstly, free-tropospheric saturation moist static energy may decrease as a region is cooled, depending on whether the cooled region is convectively coupled in the control simulation [see Figure 2c in W23]. This may allow regions which have a weakly negative instability index (just outside the convective margins) to become convectively coupled, thereby increasing the ascent fraction. This is outweighed by the second effect, in which the cooled region may itself become convectively decoupled, reducing the ascent fraction. This can be seen by removing the directly warmed/cooled region from the analysis: the ascent region instead expands (Figure S2 in Supporting Information S1). For the patch which is in a descending region (220°E; see Figure S1d in Supporting Information S1), SST warming does not strongly affect ascent fraction over the range of SST perturbations (Figure 1d).

Below we introduce a conceptual model for ascent fraction to interpret cloud responses in contrasting circulation regimes under the large-scale circulation changes shown in Figure 1.

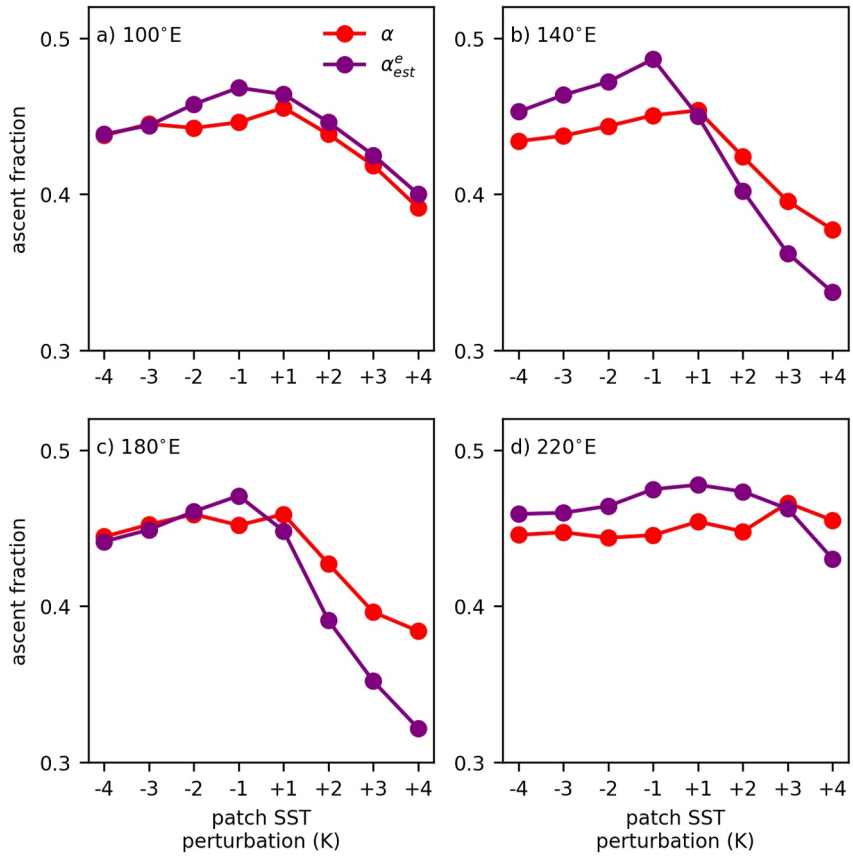

Figure 1. Ascent fraction (α, red lines)—defined as the fraction of the tropical domain (20°S to 20°N) with negative (ascending) vertical velocity at 500 hPa over the climatological year, calculated at a monthly frequency—and estimated ascent fraction adjusted for entrainment (α^e_{est}, purple lines, see Section 3.2 for details) vs. SST perturbation for patches centered at different longitudes: (a) 100°E; (b) 140°E; (c) 180°E; and (d) 220°E.

3.1. Conceptual Model

We build on the convective instability framework of W23 by further postulating that the tropical ascent fraction equals the area-weighted fraction of gridpoints where the near-surface MSE, h_{sfc}, is greater than the saturation MSE at 500 hPa, h^*_{500}. We define an instability index $[\Phi]_{i,j} = [h_{sfc}]_{i,j} - [h^*_{500}]_{i,j}$ to assess whether a given gridpoint (with latitude and longitude indices i,j, respectively) is ascending or descending. If $[\Phi]_{i,j} \geq 0$ we assume the vertical velocity at 500 hPa is negative (i.e., ascending); if $[\Phi]_{i,j} < 0$ we assume air is descending. The advantages of using a MSE-based instability index include that MSE is a conserved quantity, it provides insight into physical mechanisms and that its distribution has been found to be approximately invariant under warming (I. N. Williams & Pierrehumbert, 2017).

We test this conceptual model in the control simulation and find that it overestimates the ascent fraction as calculated with monthly data across the year ($\alpha_{est} = 0.72$ compared to the simulated value of $\alpha = 0.48$; see blue and red horizontal lines in Figure 2a). Despite this overestimation, the index shows roughly similar spatial patterns compared to 500 hPa vertical velocity and a similar seasonal cycle (Figures 2a and 2b). Descending yet unstable—according to the instability index—gridpoints have lower tropospheric MSE than those which are unstable and ascending, primarily due to lower specific humidity [not shown]. This suggests a potential role for dry-air entrainment (e.g., Singh & O'Gorman, 2013): For an ascending air parcel entraining dry air from the surrounding environment, a larger h_{sfc} would generally be required to achieve convective neutrality compared to scenario of strict convective equilibrium.

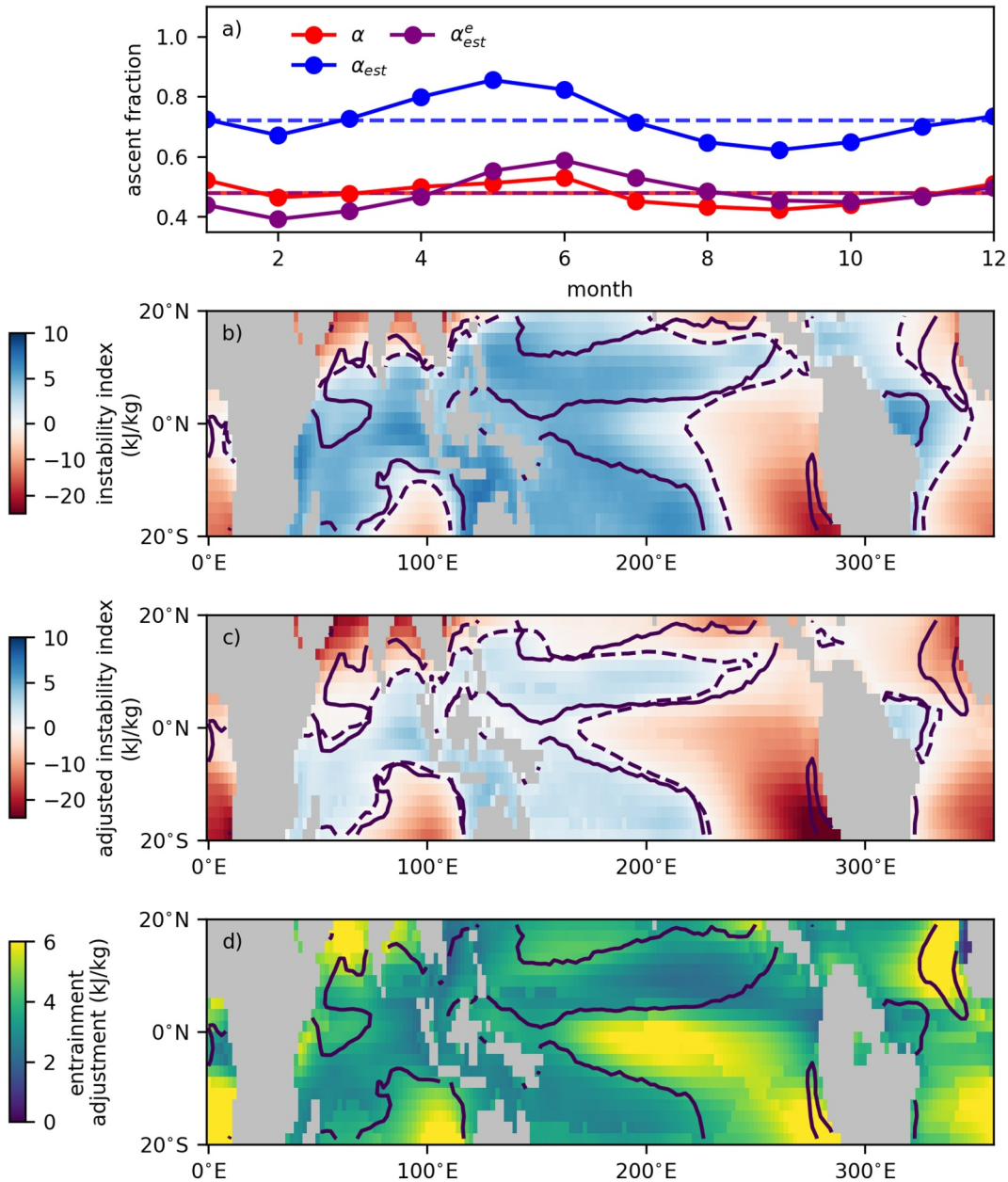

Figure 2. (a) Seasonal cycle of control simulation climatological monthly values of simulated ascent fraction (α; red markers) and estimated ascent fraction calculated without (α_{est}; blue markers) and with (α^e_{est}; purple markers) an entrainment adjustment. Also shown with corresponding horizontal lines are the ascent fractions as calculated on a monthly frequency over 12 months. Note that the entrainment parameter is chosen such that the red and purple horizontal lines are equal (see Text S2 in Supporting Information S1). (b) Instability index, Φ, for February of the control simulation (color scale) including the zero contour marked as a dashed line. The zero contour of vertical velocity at 500 hPa is also shown (solid line). (c) as for (b) but showing the entrainment-adjusted instability index, Φ^e. (d) Entrainment-adjustment, $\hat{\epsilon}h^{*e}$, for the same month (color scale) with the zero contour of vertical velocity as in (b).

3.2. Dry-Air Entrainment

To adapt the instability index to account for dry-air entrainment we turn to the zero-buoyancy plume (ZBP) model for an ensemble of convective clouds introduced by Singh and O'Gorman (2013) and subsequently found to well approximate observed stability-humidity relationships in the tropics (Palmer & Singh, 2024). This model considers an ascending plume that entrains unsaturated air from the surrounding environment. Assuming the plume is

saturated above cloud base, that it is neutrally buoyant with respect to its environment, and by using hydrostatic balance and the ideal gas law, we re-write their Equation 2 into pressure co-ordinates (Text S1 in Supporting Information S1):

$$\frac{dh^*}{dp} = -\frac{\hat{\epsilon}}{p\ln(p/p_0)}\frac{T_v(p)}{\{T_v(p)\}}L_v[q^*(p) - q(p)], \quad (1)$$

where L_v is the latent heat of vapourization, $\hat{\epsilon}$ is the entrainment parameter (Holloway & Neelin, 2009), T_v is the virtual temperature and $\{T_v(p)\} \equiv \int_{p_0}^{p}(T_v/p)\,dp/\int_{p_0}^{p}(1/p)dp$ is a vertical temperature inversely weighted by pressure between pressure levels p_0 and p.

We use the ZBP model to estimate the effect of entrainment on the MSE—proportional to the saturation deficit $[q^*(p) - q(p)]$—of a dilute parcel lifted from the sub-cloud layer to the free troposphere. We integrate Equation 1 between the lifted condensation level (LCL) and 500 hPa for each gridpoint in the control simulation to estimate the dilution of MSE during ascent due to dry-air entrainment, denoted $\hat{\epsilon}[h^{*e}]_{i,j}$. The influence of entrainment is assumed to be zero below the LCL, consistent with Singh and O'Gorman (2013). We then define an entrainment-adjusted instability index, $[\Phi^e]_{i,j} = [h_{sfc}]_{i,j} - \hat{\epsilon}[h^{*e}]_{i,j} - [h^*_{500}]_{i,j}$, such that a gridpoint is deemed to be unstable only if its near-surface MSE minus the entertainment adjustment is greater than the saturation MSE at 500 hPa. The area-weighted proportion of the domain with $\Phi^e > 0$ gives the estimated ascent fraction, subsequently denoted as α^e_{est}. We estimate the entrainment parameter $\hat{\epsilon}$ to be 0.18, with this value obtained by minimizing—over 12 months—the difference between the estimated and simulated ascent fractions in the control simulation as calculated at a monthly frequency (Figure 2a, Text S2 in Supporting Information S1). The entrainment parameter is assumed to remain constant in the perturbation simulations and is used in all subsequent analyses.

The adjusted instability index performs better in identifying ascending gridpoints (Figure 2) and is able to capture the slight contraction of ascent with cooling (Figure 1). Furthermore, inclusion of the entrainment adjustment improves estimates of the spatial pattern of ascent regions in the control simulation (Figure 2c) and the amplitude of the tropical-mean seasonal cycle (Figure 2a). Finally, the spatial pattern of the entrainment adjustment ($\hat{\epsilon}h^{*e}$) is broadly what we expect (Figure 2d), with large values in dry subsiding regions (e.g., south of the equator in the central Pacific) where we expect the saturation deficit to be highest, and small values in convective regions (e.g., the west Pacific).

Having developed the adjusted instability index using the control simulation, we now test to what extent it describes changes in ascent fraction in the perturbation simulations. We find α^e_{est} qualitatively captures the differing responses of ascent fraction to warming and cooling across patch locations (purple lines, Figures 1a–1d): there is narrowing of ascent regions with SST warming for perturbations centered on 100°E, 140°E, and 180°E, but little change for 220°E. That the index is able to replicate simulated changes in ascent fraction suggests it is a useful metric for interpreting the circulation and cloud responses to SST patch warming in different regions.

We probe the roles of two dynamical aspects on the changes in ascent fraction. First, the key role of entrainment: Including entrainment in the instability index derived from perturbation simulations—as in the control simulation—both reduces overestimation of ascent fraction (Figure S3 in Supporting Information S1) and improves estimates of the spatial extent of the ascent region (Figure S4 in Supporting Information S1). We note that the spatial distribution of $\hat{\epsilon}h^{*e}$ in the perturbation simulations (Figure S4 in Supporting Information S1) with respect to the control (Figure 2d) is similar, and that using the control simulation $\hat{\epsilon}h^{*e}$ for calculating Φ^e does not substantially alter our estimates of ascent fraction (Figure S3 in Supporting Information S1). This suggests that while including entrainment in our index is crucial for improving estimates of ascent fraction, changes in the magnitude and spatial distribution of this term are of secondary importance relative to changes in MSE at the surface and in the free troposphere. Second, we test the WTG assumption which is implicit in our MSE framework for estimating ascent fraction. We find that the estimated ascent fraction calculated using a "perfect WTG" index is very similar to our α_{est} metric (Text S3, Figure S3 in Supporting Information S1), suggesting that the assumption is sufficient, though it breaks down somewhat under cooling scenarios.

We now use our MSE framework for estimating ascent fraction to address the following question: How are changes in cloud radiative effect linked to circulation responses across regimes given the changes in large-scale ascent?

4. Cloud Responses in Changing Circulation Regimes

We begin by applying the instability index developed in Section 3 to gain insight into how ascent fraction responds to localized SST warming and cooling. We then extend this approach to decompose changes in tropical-mean CRE into contributions from different circulation regimes as defined by the instability index. In subsequent analyses we focus on two patches, those centered at 180°E and 220°E (the simulations with 100°E and 140°E patches show similar behaviors to the 180°E patch simulations) chosen for their contrasting instability profiles (cf. red lines in Figures 3a and 3b): The 180°E patch has a sharp peak in the unstable regime while the 220°E patch has a much broader peak, encompassing many more stable points.

Binning simulation data into joint distributions as a function of instability index in both the control and perturbation simulations (Figures 3a and 3b), we visualize how the prescribed SST patch warmings impact large-scale circulation by assuming that the instability index correctly identifies regions of ascent (see Section 3). We focus on the +2 K perturbations as these simulations show the largest contrast between the patches (Figures 1c and 1d), with the −2 K perturbation simulations shown in Figure S5 of Supporting Information S1 for comparison.

The instability space is split into four quadrants classified by whether the gridpoints are ascending or descending according to our instability index.

- *Subsidence regime:* gridpoints which are stable (negative instability index) in the control and perturbation simulations (Figures 3a, 3b, 3e and 3f, bottom left quadrant);
- *Convective regime:* gridpoints which are unstable in both the control and perturbation simulations (Figures 3a, 3b, 3e and 3f, top right quadrant);
- *Convective margins regime:* gridpoints which are unstable in the control but stable in the perturbation simulation (Figures 3a, 3b, 3e and 3f, bottom right quadrant);
- *Subsidence margins regime:* gridpoints which are stable in the control but unstable in the perturbation simulation (Figures 3a, 3b, 3e and 3f, top left quadrant).

The degree of spread in the joint distributions around the 1:1 line of Figures 3a, 3b is a measure of how the SST patch warming changes the instability index: a gridpoint lying on this line indicates that its instability index is unchanged between the control and perturbation simulations. Local effects of surface warming can be approximately interpreted as the spread around the 1:1 line above the portions of the x-axes corresponding to the patch instability PDFs in the control simulation (red lines, right y-axes). These can be observed in both patches. In contrast, remote effects are clearly evident for the 180°E patch simulation (Figure 3a) through the spread around the 1:1 line remote from where the warming is being applied in instability space. This spread is substantially reduced for the 220°E patch (Figure 3b). An exact separation between directly warmed and remote gridpoints is shown in Figure S6 of Supporting Information S1.

The upped-ante effect of Neelin et al. (2003) can be easily identified in our framework: For the 180°E case (Figure 3a), our estimate of ascent fraction change is driven by a greater area moving from unstable to stable ("convective margins") after the perturbation than vice versa ("subsidence margins"). The convective margins quadrant is associated with strong increases in Δh^*_{500} for the 180°E patch—in contrast to the 220°E patch (Figures S7a and S7b in Supporting Information S1)—which outpace increases in near-surface MSE and therefore becoming stable according to our index.

4.1. Cloud Responses in Different Circulation Regimes

We now leverage our framework to analyze the cloud responses in the different circulation regimes (Figures 3e–3h). Integrating the changes in net cloud radiative effect ($\Delta \mathrm{CRE}_{net}$) across the tropical domain for each SST perturbation results in negative changes that are strongly nonlinear with respect to the SST change and are larger for the 180°E patch compared to the 220°E patch (Figures 3g and 3h; as shown by W23). Three of the above-identified regimes contribute substantially to the changes in cloud radiative effect for the 180°E patch (Figure 3g). We discuss each of these regions in turn and assess vertical profiles of changes in cloud properties in

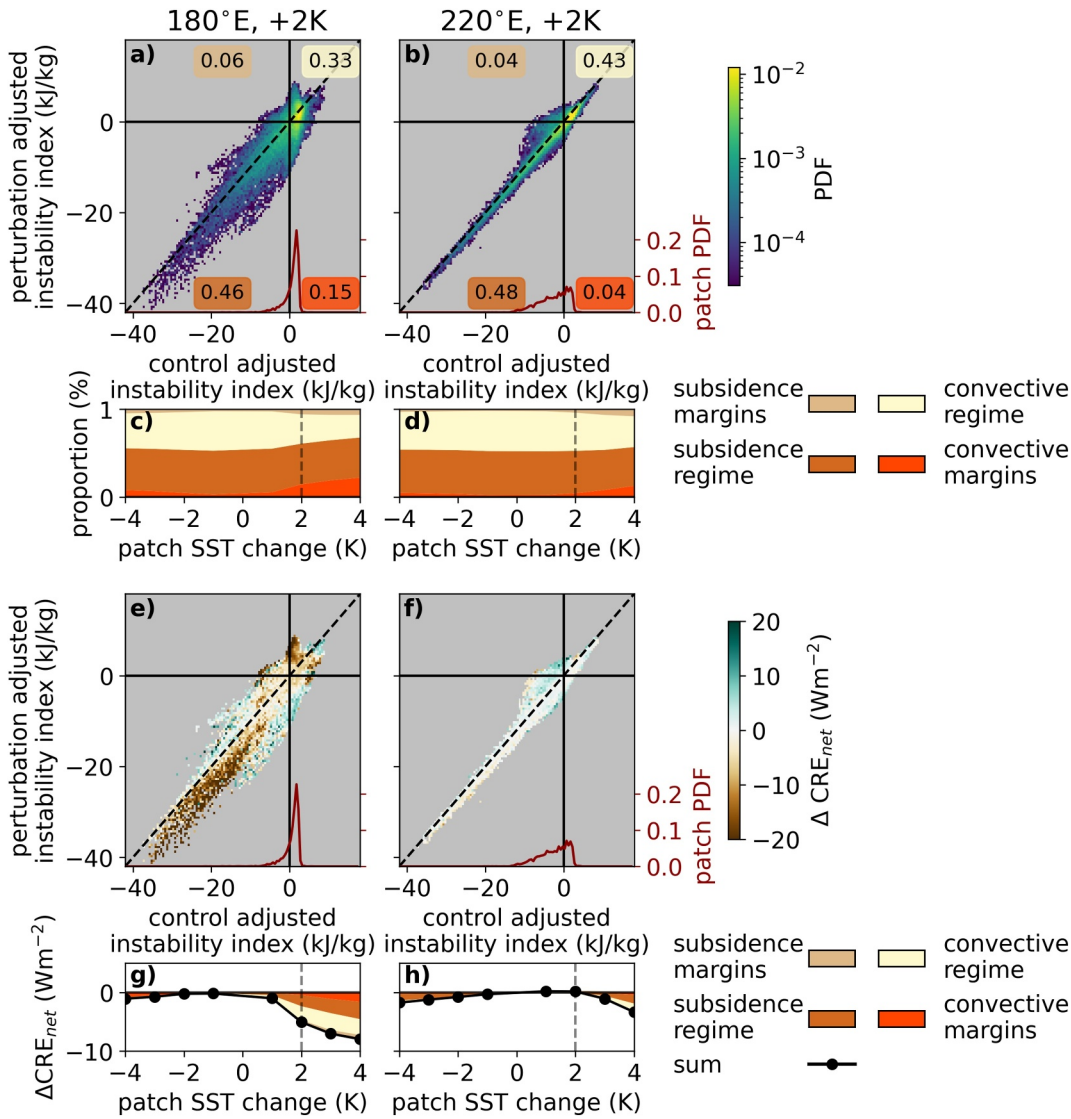

Figure 3. (a, b): Joint distributions of the entrainment-adjusted instability index in the control (*x*-axes) and +2 K perturbation simulations (*y*-axes) for warming patches centered at (a) 180°E and (b) 220°E. The colorscale indicates the density of each bin. Red lines and right hand *y*-axes show the control instability index distribution directly above the patch. (c, d): For all SST perturbations, the proportion of the domain falling within each quadrant. Quadrants are defined as "convective regime" [top-right of (a, b)]; "subsidence regime" [bottom-left]; "convective margins regime" [bottom-right]; and "subsidence margins regime [top-left]. (e, f): As for (a, b), but here the colorscale indicates the change in net cloud radiative effect (ΔCRE_{net}) in instability index space. (g, h): Area-weighted contributions from each quadrant in (e, f) to the tropics-wide change in net cloud radiative effect for each SST perturbation (black lines indicate the total changes).

subsets of the identified regimes (Figure S8 in Supporting Information S1). The locations of selected gridpoints are shown in Figure 4.

First, for the 180°E patch the low cloud effects in climatological subsidence regimes are readily identifiable. As expected, the strongly negative change in net cloud radiative effect is driven by shortwave effects (Figure S9 in Supporting Information S1) and is remote from where the SST warming is applied (Figure S6 in Supporting Information S1). This regime is much reduced in the 220°E case. Focusing explicitly on the gridpoints with a negative ΔCRE_{net}, we confirm that there is an increase in cloud fraction in the lower troposphere (below ~700 hPa) from increasing cloud liquid water (Figure S8a in Supporting Information S1), consistent with increases in low cloud (see Section 1). There is also a substantial decrease in high cloud fraction (above ~500 hPa), driven by a reduction in cloud ice, though the processes behind this are unclear.

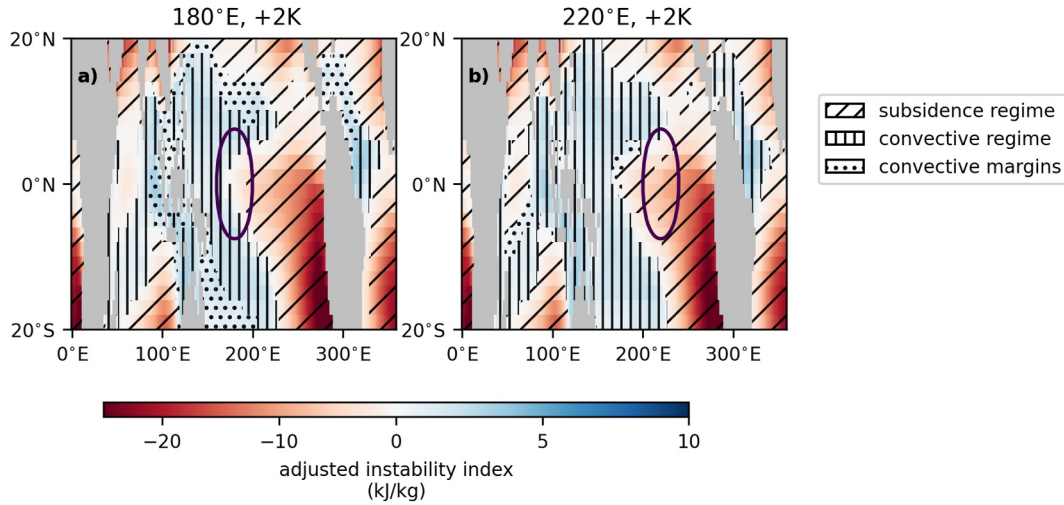

Figure 4. (a) Adjusted instability index (colors) in February for the control simulation. Purple contour indicates region where SSTs have been warmed by ≥0.4 K in the +4 K simulation for the warming patch centered at 180°E. Hatching shows gridpoints identified to be in the subsidence (diagonal hatching) regime, convective regime (vertical hatching), or convective margins regime (dotted hatching) (see main text for definitions) after the +2 K perturbation. (b) As (a), but here showing results for perturbation simulation with a +2 K SST warming patch centered at 220°E.

The second regime of interest is the convective region (Figure 4), a regime contributing substantially to the overall negative trend in ΔCRE_{net} (Figures 3g and 3h). Convective regime gridpoints directly warmed by the SST increase have changes to their cloud profiles that are distinct compared to cloud changes in remote convective regime regions. For gridpoints directly warmed these cloud changes are straightforward, with a large increase in both cloud liquid water in the lower troposphere and cloud ice in the upper troposphere consistent with increases in cloud fraction above the boundary layer (Figure S8b in Supporting Information S1). This suggests an increase in the area fraction of deep convective cores of anvil clouds, which corresponds to the negative ΔCRE_{net} associated with this regime (Figures S6a and S6b in Supporting Information S1). These cloud profile changes are also present in the 220°E case, albeit reduced. For convective regime gridpoints which are not directly warmed in the 180°E case, the cloud changes are more subtle, with some evidence of high clouds contracting and rising as well as an increase in low- and mid-level clouds (Figure S8c in Supporting Information S1). These remote changes to convective regimes are also associated with a strongly negative ΔCRE_{net}, and only evident for the warmest SST perturbations for the 220°E patch (Figures S6e–S6h in Supporting Information S1).

The final regime we discuss includes points at the convective margins in the control simulation which become stable to convection in response to SST warming (Figures 3 and 4). These points overall contribute a relatively small proportion of the negative trend of ΔCRE_{net} for the 180°E patch, but show a direct link between cloud radiative response and ascent fraction change. These radiative effects, primarily longwave, are somewhat offset by shortwave effects (Figure S9 in Supporting Information S1) and are associated with a substantial decrease in high ice clouds, with decreases extending through the mid-troposphere (to ∼600 hPa) and increases in low cloud (Figure S8d in Supporting Information S1). We note that the decrease in low cloud cover in these convective margin regimes is consistent with other studies which have used a patch warming approach centered on the western Pacific (Dong et al., 2019). These effects are reduced in the 220°E case.

5. Conclusions and Discussion

Here we extend the framework of W23 to decompose cloud responses to localized patch warmings by circulation regime. We develop an instability index which incorporates the effects of dry-air entrainment into ascending air and broadly captures changes in tropical-mean ascent fraction across the perturbation. The instability index is then applied to interpret cloud radiative effect changes induced by the patch warming.

Warming concentrated in ascending regions efficiently raises saturation MSE in the free troposphere and generates remote effects. A well-studied remote effect is in climatologically subsiding regions associated with

increased static stability and low-cloud amount, and changes in tropical-mean cloud radiative effect (e.g., Andrews & Webb, 2018; Dong et al., 2019; Rugenstein et al., 2023; Zhou et al., 2016). This response is readily identified in our framework. However, our framework also reveals contributions from other circulation regimes in response to patterned warming. In the case of warming in ascending regions, direct heating intensifies climatological ascent leading to substantial increases in thick convective cloud producing a negative change in cloud radiative effect. The effects of warming are also seen in ascending regions not directly warmed at the surface, with small increases in mid- and low-level clouds. Finally, the raising of the convective threshold reduces the tropical ascent fraction—the convective margins quadrant in our analysis—consistent with previous studies (Byrne & Schneider, 2016; Jenney et al., 2020; Neelin et al., 2003; Su et al., 2020). These convective margins experience a reduction in high cloud and increase in low cloud associated with a small but notable contribution to the tropical-mean change in cloud radiative effect.

While some of the cloud changes discussed may be considered thermodynamic in nature—driven by increases in temperature—they arise through dynamic effects: first through vertical coupling in ascending regions, which narrow with warming, and second through the influence of WTG in the free troposphere. We argue that the effects of changing circulation in modulating the cloud response to patterned warming thus far have not received sufficient attention. Our work has shown complexity in cloud responses in different regions, and further work is required to understand these more fully. In particular, there are interesting questions about the dynamics of the pattern effect which warrant further study.

Firstly, our work demonstrates the role of dry-air entrainment in the large-scale circulation changes associated with patterned SST warming and raises potential avenues for future research: What range of entrainment parameters are estimated by GCMs and can a similar approach be used with observations? To what extent does the spatial distribution of the saturation deficit vary with patterned warming in different models?

Secondly, while we find that the assumption of WTG in the tropical free troposphere is largely sufficient for our simple conceptual model of ascent fraction, an interesting feature emerges: there are subsiding regimes in the control simulation where free tropospheric MSE does not increase in line with the WTG assumption and instead decreases with warming (Figure S7 in Supporting Information S1), with neutral or weakly positive changes in cloud radiative effects associated with these spatially non-uniform changes (Figure 3). The location of SST warming is implicated in this spatial heterogeneity in free tropospheric warming through thermodynamic and dynamic processes. In particular, dissipative processes work to constrain tropospheric warming to the region of surface warming (Keil et al., 2023), and elucidating the role of non-WTG effects on top-of-atmosphere radiation fluxes would be an interesting avenue for further study.

Finally, the open question of whether these effects can be identified in more realistic warming scenarios, or indeed observations, remains. Disentangling the effects of warming patterns from global-mean temperature changes on large-scale circulation and cloud changes is challenging, making insights from idealized modeling studies such as these important in establishing mechanisms under controlled conditions.

Data Availability Statement

The simulation data used for the study are openly available at https://zenodo.org/records/7621085 (A. I. L. Williams, 2022). Software used for analysis is preserved at https://zenodo.org/records/14277199 (Mackie, 2024).

Acknowledgments
AM and MB acknowledge funding from the UK Natural Environment Research Council (Grant NE/T006269/1) and thank Peter Hill, Chris Holloway, Hugo Lambert, Monisha Natchair, Danny McCulloch, Mark Webb, and two anonymous reviewers for helpful discussions and suggestions. EV acknowledges funding from the UK Natural Environment Research Council, Doctoral Training Partnership in Environmental Research (Grant NE/S007474/1). AW acknowledges funding from the CIMES Postdoctoral Fellowship under award NA18OAR4320123 from the National Oceanic and Atmospheric Administration, U.S. Department of Commerce.

References

Andrews, T., Gregory, J. M., Paynter, D., Silvers, L. G., Zhou, C., Mauritsen, T., et al. (2018). Accounting for changing temperature patterns increases historical estimates of climate sensitivity. *Geophysical Research Letters*, *45*(16), 8490–8499. https://doi.org/10.1029/2018GL078887

Andrews, T., & Webb, M. J. (2018). The dependence of global cloud and lapse rate feedbacks on the spatial structure of tropical Pacific warming. *Journal of Climate*, *31*(2), 641–654. https://doi.org/10.1175/JCLI-D-17-0087.1

Armour, K. C., Proistosescu, C., Dong, Y., Hahn, L. C., Blanchard-Wrigglesworth, E., Pauling, A. G., et al. (2024). Sea-surface temperature pattern effects have slowed global warming and biased warming-based constraints on climate sensitivity. *Proceedings of the National Academy of Sciences*, *121*(12), e2312093121. https://doi.org/10.1073/pnas.2312093121

Barsugli, J. J., & Sardeshmukh, P. D. (2002). Global atmospheric sensitivity to tropical SST anomalies throughout the Indo-Pacific basin. *Journal of Climate*, *15*(23), 3427–3442. https://doi.org/10.1175/1520-0442(2002)015⟨3427:GASTTS⟩2.0.CO;2

Bony, S., Dufresne, J.-L., Le Treut, H., Morcrette, J.-J., & Senior, C. (2004). On dynamic and thermodynamic components of cloud changes. *Climate Dynamics*, *22*(2), 71–86. https://doi.org/10.1007/s00382-003-0369-6

Byrne, M. P., Pendergrass, A. D., Angeline, G., Wodzicki, K. R., & Wodzicki, K. R. (2018). Response of the Intertropical Convergence Zone to climate change: Location, width, and strength. *Current Climate Change Reports*, *4*, 355–370. https://doi.org/10.1007/s40641-018-0110-5

Byrne, M. P., & Schneider, T. (2016). Narrowing of the ITCZ in a warming climate: Physical mechanisms. *Geophysical Research Letters*, *43*(21), 11350–11357. https://doi.org/10.1002/2016GL070396

Byrne, M. P., & Schneider, T. (2018). Atmospheric dynamics feedback: Concept, simulations, and climate implications. *Journal of Climate*, *31*(8), 3249–3264. https://doi.org/10.1175/JCLI-D-17-0470.1

Dong, Y., Proistosescu, C., Armour, K. C., & Battisti, D. S. (2019). Attributing historical and future evolution of radiative feedbacks to regional warming patterns using a Green's Function approach: The preeminence of the Western Pacific. *Journal of Climate*, *32*(17), 5471–5491. https://doi.org/10.1175/JCLI-D-18-0843.1

Duffy, M. L., & O'Gorman, P. A. (2023). Intermodel spread in Walker circulation responses linked to spread in moist stability and radiation responses. *Journal of Geophysical Research: Atmospheres*, *128*(1), e2022JD037382. https://doi.org/10.1029/2022JD037382

Emanuel, K. A., David Neelin, J., & Bretherton, C. S. (1994). On large-scale circulations in convecting atmospheres. *Quarterly Journal of the Royal Meteorological Society*, *120*(519), 1111–1143. https://doi.org/10.1002/qj.49712051902

Fueglistaler, S. (2019). Observational evidence for two modes of coupling between sea surface temperatures, tropospheric temperature profile, and shortwave cloud radiative effect in the tropics. *Geophysical Research Letters*, *46*(16), 9890–9898. https://doi.org/10.1029/2019GL083990

Giorgetta, M. A., Brokopf, R., Crueger, T., Esch, M., Fiedler, S., Helmert, J., et al. (2018). ICON-A, the atmosphere component of the ICON Earth System Model: I. Model description. *Journal of Advances in Modeling Earth Systems*, *10*(7), 1613–1637. https://doi.org/10.1029/2017MS001242

Hill, P. G., Holloway, C. E., Byrne, M. P., Lambert, F. H., & Webb, M. J. (2023). Climate models underestimate dynamic cloud feedbacks in the tropics. *Geophysical Research Letters*, *50*(15), e2023GL104573. https://doi.org/10.1029/2023GL104573

Holloway, C. E., & Neelin, J. D. (2009). Moisture vertical structure, column water vapor, and tropical deep convection. *Journal of the Atmospheric Sciences*, *66*(6), 1665–1683. https://doi.org/10.1175/2008JAS2806.1

Jenney, A. M., Randall, D. A., & Branson, M. D. (2020). Understanding the response of tropical ascent to warming using an energy balance framework. *Journal of Advances in Modeling Earth Systems*, *12*(6), e2020MS002056. https://doi.org/10.1029/2020MS002056

Keil, P., Schmidt, H., Stevens, B., Byrne, M. P., Segura, H., & Putrasahan, D. (2023). Tropical tropospheric warming pattern explained by shifts in convective heating in the Matsuno–Gill model. *Quarterly Journal of the Royal Meteorological Society*, *149*(756), 2678–2695. https://doi.org/10.1002/qj.4526

Mackie, A. (2024). Climate-Dynamics-Lab/responses_patterned_warming: December 4th, 2024 release (version 1.3) [Software]. *Zenodo*. https://doi.org/10.5281/zenodo.14277199

Mackie, A., Brindley, H. E., & Palmer, P. I. (2021). Contrasting observed atmospheric responses to tropical sea surface temperature warming patterns. *Journal of Geophysical Research: Atmospheres*, *126*(7), e2020JD033564. https://doi.org/10.1029/2020JD033564

Mackie, A., & Byrne, M. P. (2023). Effects of circulation on tropical cloud feedbacks in high-resolution simulations. *Journal of Advances in Modeling Earth Systems*, *15*(5). https://doi.org/10.1029/2022MS003516

Neale, R., & Hoskins, B. (2000). A standard test for AGCMs including their physical parametrizations: I: The proposal. *Atmospheric Science Letters*, *1*(2), 101–107. https://doi.org/10.1006/asle.2000.0019

Neelin, J. D., Chou, C., & Su, H. (2003). Tropical drought regions in Global warming and El Niño teleconnections. *Geophysical Research Letters*, *30*(24). https://doi.org/10.1029/2003GL018625

Palmer, L. A., & Singh, M. S. (2024). The horizontal and vertical controls on the thermal structure of the tropical troposphere. *Quarterly Journal of the Royal Meteorological Society*, *150*(765), 5548–5560. https://doi.org/10.1002/qj.4888

Rugenstein, M., Zelinka, M., Karnauskas, K. B., Ceppi, P., & Andrews, T. (2023). Patterns of surface warming matter for climate sensitivity. *EOS*, *104*. https://doi.org/10.1029/2023EO230411

Singh, M. S., & O'Gorman, P. A. (2013). Influence of entrainment on the thermal stratification in simulations of radiative-convective equilibrium. *Geophysical Research Letters*, *40*(16), 4398–4403. https://doi.org/10.1002/grl.50796

Sobel, A. H., & Bretherton, C. S. (2000). Modeling tropical precipitation in a single column. *Journal of Climate*, *13*(24), 4378–4392. https://doi.org/10.1175/1520-0442(2000)013⟨4378:MTPIAS⟩2.0.CO;2

Su, H., Wu, L., Zhai, C., Jiang, J. H., Neelin, J. D., & Yung, Y. L. (2020). Observed tightening of tropical ascent in recent decades and linkage to regional precipitation changes. *Geophysical Research Letters*, *47*(3). https://doi.org/10.1029/2019GL085809

Williams, A. I. L. (2022). Data from "Circus tents, convective thresholds and the non-linear climate response to tropical SST changes" [Data]. *Zenodo*. https://zenodo.org/records/7621085

Williams, A. I. L., Jeevanjee, N., & Bloch-Johnson, J. (2023). Circus tents, convective thresholds, and the non-linear climate response to tropical SSTs. *Geophysical Research Letters*, *50*(6). https://doi.org/10.1029/2022GL101499

Williams, I. N., & Pierrehumbert, R. T. (2017). Observational evidence against strongly stabilizing tropical cloud feedbacks. *Geophysical Research Letters*, *44*(3), 1503–1510. https://doi.org/10.1002/2016GL072202

Wills, R. C. J., Dong, Y., Proistosecu, C., Armour, K. C., & Battisti, D. S. (2022). Systematic climate model biases in the large-scale patterns of recent sea-surface temperature and sea-level pressure change. *Geophysical Research Letters*, *49*(17). https://doi.org/10.1029/2022GL100011

Wyant, M. C., Bretherton, C. S., Bacmeister, J. T., Kiehl, J. T., Held, I. M., Zhao, M., et al. (2006). A comparison of low-latitude cloud properties and their response to climate change in three AGCMs sorted into regimes using mid-tropospheric vertical velocity. *Climate Dynamics*, *27*(2–3), 261–279. https://doi.org/10.1007/s00382-006-0138-4

Zhou, C., Zelinka, M. D., & Klein, S. A. (2016). Impact of decadal cloud variations on the Earth's energy budget. *Nature Geoscience*, *9*(12), 871–874. https://doi.org/10.1038/ngeo2828